Optik - International Journal for Light and Electron Optics 192 (2019) 162870

Contents lists available at ScienceDirect

Optik

journal homepage: www.elsevier.com/locate/ijleo

Original research article

Optical Camera Communication system for three-dimensional indoor localization

Patricia Chavez-Burbano[a,b,*], Victor Guerra[b], Jose Rabadan[b], Rafael Perez-Jimenez[b]

[a] Escuela Superior Politcnica del Litoral, ESPOL, Facultad de Ingeniera en Electricidad y Computacion, Campus Gustavo Galindo Km 30.5 Via Perimetral, P.O. Box 09-01-5863, Guayaquil, Ecuador

[b] Institute for Technological Development and Innovation in Communications (IDeTIC), ULPGC, Las Palmas, Spain

ARTICLE INFO

Keywords:
Indoor Positioning System
Optical Camera Communication
Image processing
Industrial internet of things

ABSTRACT

Nowadays, indoor localization methods are intensively researched due to their potential use in location-based services, robots' navigation and applications for Industrial Internet of Things (IIoT). The tendency of including small devices with Light Emitting Diodes (LED) for decoration purposes and the emergence of better low-cost cameras in the market, impulse the use of Optical Camera Communication (OCC) for Indoor Positioning Systems (IPS). In this work a real-time two-step 3D Indoor Positioning System for multiple devices using OCC and LED beacons is proposed. The beacons are positioned at a predefined static distance from the camera, forming a virtual reference plane that represents the frame of the real world elements' positions captured in a photo. A simplified version of the trigonometric equations for transforming 2D pixel projection into real distances is applied to obtain the vertical and horizontal separation between the objects and the beacons. While the relation of the beacons' and the objects' projection size is used to determine the distance of each object to the camera. These distances together allowed to calculate the 3D location of the elements by trilateration. Experimental validation of the method was performed, and the results showed a mean location error of 1.24 cm for the three dimensions with an average process time of 18.2 ms per frame for four simultaneous targets correctly identified, at a distance of 2.00 m.

1. Introduction

The increasing trend of implementing location-based services and applications (e.g., indoor navigation or opportunistic marketing) requires more accurate Indoor Positioning Systems (IPS). However, Global Positioning System (GPS) is not an accurate option for indoor localization [1]. Alternative solutions based on Wireless Fidelity (WiFi), Bluetooth, Radio Frequency (RF), Ultra-Wide Band (UWB), Infra-Red, and Visible Light Communication (VLC) have been proposed [2,3]. Among all these techniques, VLC [4] provides high positioning accuracy (PA), energy efficiency and can be easily and almost inexpensively implemented, while offering immunity to traditional RF interference. VLC takes advantage of the promoted replacement of conventional lighting systems with LED-based devices and the introduction of these elements for decoration purposes.

Visible Light Positioning (VLP) techniques can be classified in several ways. In [5] these techniques were separated into two main groups: direct positioning and two-step localization. The direct positioning techniques are usually highly complex and lead to optimal

* Corresponding author at: Escuela Superior Politcnica del Litoral, ESPOL, Facultad de Ingeniera en Electricidad y Computacion, Campus Gustavo Galindo Km 30.5 Via Perimetral, P.O. Box 09-01-5863, Guayaquil, Ecuador.
E-mail address: paxichav@espol.edu.ec (P. Chavez-Burbano).

https://doi.org/10.1016/j.ijleo.2019.05.076
Received 28 February 2019; Received in revised form 20 May 2019; Accepted 23 May 2019

solutions without previous parameter estimation [6,7]. The two-step localization relays on a first stage for data extraction, which is then used for estimating the position in a less complex second stage that gives suboptimal results [8,9]. Based on this analysis, a real-time IPS should be implemented as a two-step localization method to avoid high data storage requirements, computing intensive algorithms and elevated computational delays. Another VLP techniques classification was presented in [10], where the methods were divided into five groups: proximity, fingerprinting, triangulation, vision analysis, and hybrid algorithms. The proximity [11], fingerprinting [12,13] and triangulation [14–16] methods use photodiodes (PD) as receivers, and require a multiplexing process. While, vision analysis techniques use cameras as receivers and do not need the multiplexing stage. However, the hybrid algorithms [17,18] use photodiodes or cameras as receivers, and the multiplexation is optional. Since the PD are susceptible to the light beam direction limiting their use with mobile objects, the image sensors can spatially separate light sources and cameras with better resolution have been already included inside the buildings for security reasons, the vision analysis VLP techniques should be exploited.

In 2012 a specialized device that determines its three-dimensional (3D) location based on trigonometric calculations by using two embedded cameras and four external beacons was patented [19]. The beacons' position and the distance between the cameras were known, so the central point of the device, corresponding to the object's 3D location, was calculated by comparing the captured images. Luxapose, an VLP system introduced in [20], calculated the position of a smartphone based on scaling factors by using its camera and beacons, each one with different frequencies. This positioning algorithm reached an average location error of 10 cm. In [21], the use of neural networks for avoiding complex mathematical models in the translation from real-world distances to images pixels projections was proposed. This approach reported an error of 1 cm at a distance of 10 cm but increased to 20 cm at 2 m; and consumed computational resources and time. The VLP proposed in [22] used wearables with embedded cameras (e.g., smart glasses, watch) and polarized the beacons. Then the orientation and location of the lights were extracted from the camera's video and the device's position was calculated by implementing an Angle of Arrival (AOA) algorithm. The average location's error was 30 cm with a 1.8 s delay working at 300 MHz. In [23], the use of the camera along with the accelerometer sensor of a mobile allowed the location of the device independently of the receiver orientation. In this case, a rotation matrix based on the information given by the accelerometer is applied to the set of quadratic equations that represents the real world positions projected over the photo. The average location's error was 10 cm, even with noise reduction in the frames. Similarly, the VLP technique proposed in [24] used the camera, accelerometer, and gyroscope embedded on the smart-phones for finding the location and orientation of the mobile device. In this case, a low-complexity singular value decomposition based sensor fusion algorithm was used to enhance the PA with the data from the sensors, and the mean positioning error was reduced to 4.4 cm. An experimental demonstration of indoor VLP using image sensors was presented in [25], the position of the camera was determined from the geometrical relations of the LEDs in the images. These LEDs constantly transmitted their coordinates using Phase Shift Keying (UPSK) modulation. The mean positioning error of this VLP reached 5 cm for a distance of 1.20 m, and it increased to 6.6 cm for a height of 1.80 m. Additionally, this method was improved in [26] by grouping the LEDs into blocks with a single coordinates' emitter and implementing a back propagation Artificial Neural Network (ANN) for a roughly and precise direct estimation of the position. In this case, the mean positioning error was reduced to 1.49 cm for a height of 1.80 m with an online processing time of 0.15 s.

This work presented the two-step 3D Indoor Positioning System using Optical Camera Communication (OCC) initially introduced in the 11th International Symposium on Communication Systems, Networks Digital Signal Processing (CSNDSP2018) [27]. This system establishes the position and tracks the movements of several devices simultaneously, based on the trigonometric relations between the camera, a beacon's virtual plane parallel to the receiver's normal plane and the objects to be located. In order to improve the system's performance and show its potential applications, some changes were introduced. At first, the identification signal was set as a combination of different frequencies for each color channels instead of a simple fixed frequency. In this way, the number of simultaneous objects to be located increased significantly. Secondly, for speeding up the localization, the image processing stage was separated into two steps: beacons' identification, which was done only at the beginning; and objects' positioning. Additionally, a tracking module was included and tested.

Instead of locating an embedded camera device, the usual paradigm of OCC's VLP techniques, the proposed system employs a single camera for positioning different objects based on the identification of static beacons which location is previously known. Therefore, this scheme's implementation is economically efficient; the objects to be located and the beacons require to be equipped with relatively inexpensive LED-based devices, while a pre-existing security camera can be used for the image capture process. Due to the use of simplified trigonometric equations and the creation of the beacon's virtual plane, this procedure is less computing intensive than previous solutions while obtaining precise positions in two and three dimensions.

This paper is organized as follows: in Section 2 the fundamental elements of the system are described along with its setup; and the related processes, image processing, localization process and location management, are detailed. Section 3 presents the experimental validation of the system, including the new tracking module, analysing the image processing and positioning results of a given example. Finally, some conclusions and future works are presented in Section 4.

2. System description

As shown in Fig. 1, the proposed system employs four beacons (B_1–B_4) for the 3D indoor concurrent localization of several objects (O_n). Each device, beacons and objects, uses a small LED display for transmitting the corresponding identification signal. The receiver is a rolling shutter camera with a minimum resolution of 640 × 480 pixels. Since all the necessary hardware are commercial off-the-shelf (COTS) products, the implementation of this system is a low-cost solution.

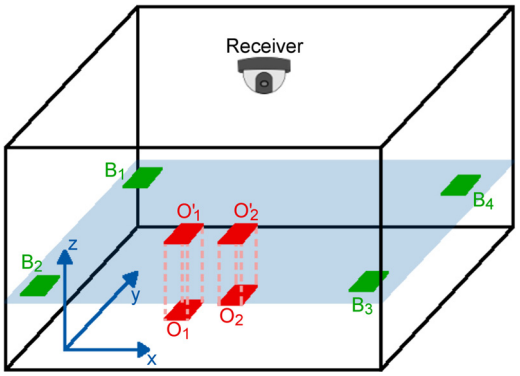

Fig. 1. Proposed system's scheme. In this example, a room with a single ceiling security camera (receiver), the four beacons (B_1–B_4) that form the virtual plane and two objects to be located (O_1 and O_2) is represented. The projected representation of the objects over the formed virtual plane (O'_1 and O'_2) are showed as they will appear in the frames.

2.1. System setup

The beacons are located at a predefined distance *D* (see Fig. 2) to the camera's normal plane forming a virtual referential plane that represents the captured image without rotations. Each beacon's position, which is not necessarily located at the corners of the room, is known beforehand by the system and accordingly has been stored for the localization process. The discrete objects can be placed in any position within the camera's angular range, including those outside the virtual plane.

All the devices transmit a fixed code, in this case '0 × AAAA', constantly using On–Off Keying (OOK) modulation at four predefined frequencies (fs_i), which selection depends on their assigned identification (ID). The beacons only use the green channel and emit at the beginning of each localization process. The objects to be located employ a combination of the red and blue channels and transmit continuously. This combination of two channels and four frequencies allows the existence of 24 simultaneous objects on our environment. A precondition of the system is that the camera has been previously calibrated and set-up to avoid lenses' distortions. The camera capture the frames at a predetermined frame per second (*fps*) value using N_V pixels of vertical resolution and send each one to a computer for its corresponding image processing. Due to the rolling shutter effect and the OOK modulation, the transmitted code can be observed in the captured images as bands, black and color, as shown in Figs. 3 and 4, which widths ($Npixels_i$) can be calculated using Eq. (1).

$$\mathrm{Npixels}_i = \frac{N_V}{\mathrm{fs}_i} \cdot \mathrm{fps} \tag{1}$$

Since the proposed system is a two-step method, it requires two separate stages for position estimation. During the first step, called Image Processing, the position related parameters are extracted directly from the frames: the beacons' location from the first one and the objects' data from the others. In the second stage, denominated Localization Process, the position of the different objects is calculated using a geometric method.

2.2. Image processing

This step started with the image binarization, denominated as procedure A in the Image Processing diagram (Fig. 5). For this process, the appropriated channel is binarized using Otsu's algorithm for thresholding [28], based on the data extracted from its histogram. For the beacons, the binarization is applied only to the first frame's green channel. In the case of the objects, the red and blue channels of each frame are processed, then both channels are combined (procedure B) to compose a unique binary image.

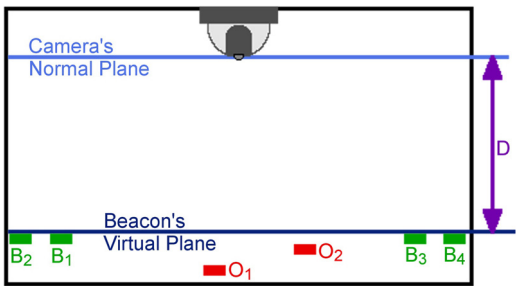

Fig. 2. Vertical cutting plane of the proposed example, showing the z-dimension position of the beacons (B_1–B_4), and the objects (O_1 and O_2), as well as, the beacon's virtual plane and the camera's normal plane.

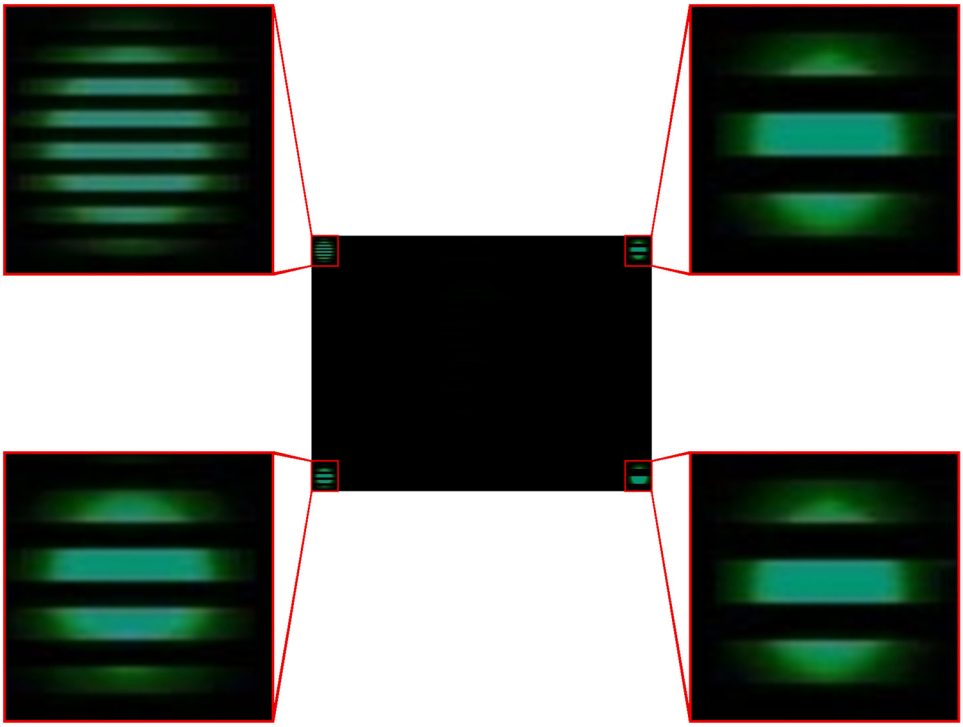

Fig. 3. Experimental image of the four beacons (B_1–B_4) extracted from the first frame. At this stage, the beacons are perceived as independent switching light sources but they have no identification labels associated.

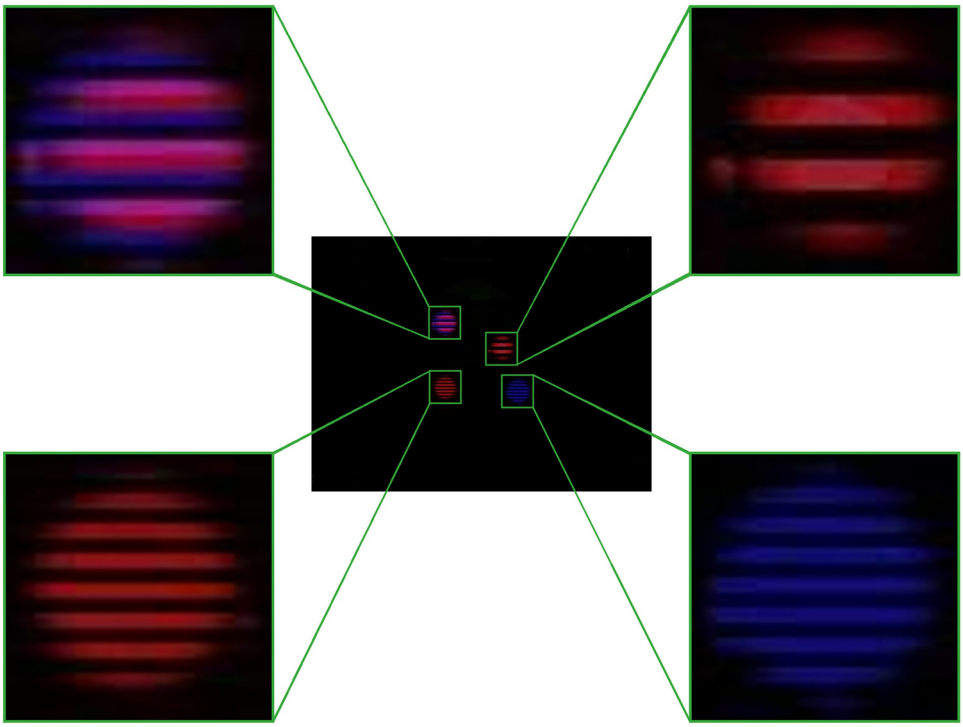

Fig. 4. Experimental image of the objects to be located simultaneously (O_1–O_4). At this stage, the objects are perceived as independent switching light sources but they have no identification labels associated.

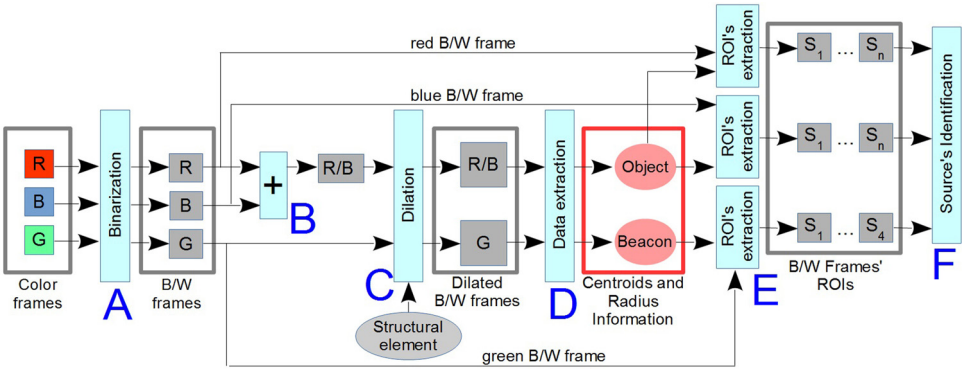

Fig. 5. Image processing flow chart. Processes are represented by light blue boxes and addressed with blue capital letters: A – Binarization, B – Combination, C – Dilation, D – Data Extraction, E – ROI's Extraction, and F – Source's Identification. (For interpretation of the references to color in this figure legend, the reader is referred to the web version of this article.)

Afterwards, the binary image is dilated (procedure C) for growing the size of the white bands symmetrically in all directions. For this purpose, the convolution between the binary image and an 8 pixels diameter binary disk, known as the structural element of this morphological operation, was used for the image dilation. After this process, the light sources (beacons or objects) can be observed as closed white regions in the resulting frame, as shown in Figs. 6 and 7. Subsequently, the centroid's coordinates and approximate radius of each source (S_1–S_4) are determined in per frame bases by processing this image (procedure D).

The appropriated channel's region of interest (ROI) of each light source is extracted from the undilated binarized image by using the centroid's location and radius information obtained from previous steps. As shown in Fig. 8, in the beacons' case, only one ROI is cut from the frame for each light source (green channel); while Fig. 9 shows that for each object to be located two ROIs are generated (red and blue channels).

To identify the different light sources (procedure F), the band's width $Npixels_i$ is calculated in each obtained ROI (Figs. 8 and 9). This width is the statistical mode of the consecutive white pixels in the three central columns of the each image's corresponding channel (green for beacons; red and blue for the objects). The switching frequency (fs_i) of each channel is obtained by using Eq. (1), where N_V and fps are known camera's settings. Since each emitter (beacons and objects) uses a unique switching frequency combination based on its identification code, the source is accordingly associated with the proper beacon or object. In this way, the pixel's horizontal and vertical location of each beacon (B_{Hi}, B_{Vi}) is matched with a known real 3D position and stored by the system along with the source diameter (d_{Bi}). Similarly, for the objects to be located, the centroid's horizontal and vertical pixel coordinates (O_{Hi}, O_{Vi}) and the source diameter (d_{Oi}) are recorded for further calculations. The light source's diameter is calculated as the maximum consecutive white pixels in the rows of the extracted ROI.

2.3. Localization process

In [29] Eqs. (2) and (3) were proposed for estimating the 2D pixel's projection (H_{img}, V_{img}) in a picture of a real distance (H_{real}, V_{real}). In these equations, D is the distance between transmitter and receiver, γ is the angle formed by the intersection of the emitter-receiver vertical plane and the emitter's normal plane; and φ is the relation between the resolution in pixels ($N_{H,V}$) and the field of view (FOV) of the selected camera: $\varphi_H = FOV_H/N_H$.

Fig. 6. Experimental dilated binary image of the four beacons extracted from the first frame. At this stage, the beacons are perceived as independent white regions and they have temporal labels (S_1–S_4) associated.

Fig. 7. Experimental combined and dilated binary image of the objects to be located simultaneously. At this stage, the objects are perceived as independent white regions and they have temporal labels (S_1–S_4) associated.

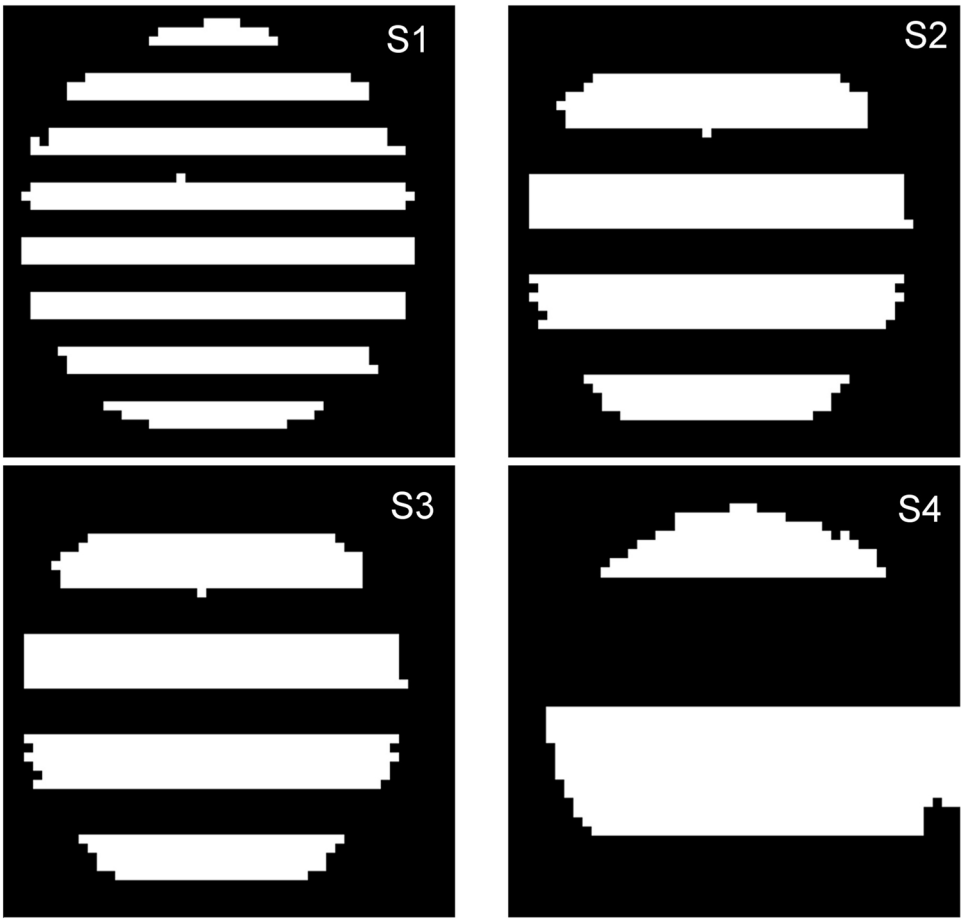

Fig. 8. Extracted binary images of the Beacons in the green channel for determining the corresponding source's code.

$$H_{\text{img}} = \frac{1}{\varphi_H}\left[\tan^{-1}\frac{H_{\text{real}}\sin\gamma}{2D - H_{\text{real}}\cos\gamma} + \tan^{-1}\frac{H_{\text{real}}\sin\gamma}{2D + H_{\text{real}}\cos\gamma}\right] \tag{2}$$

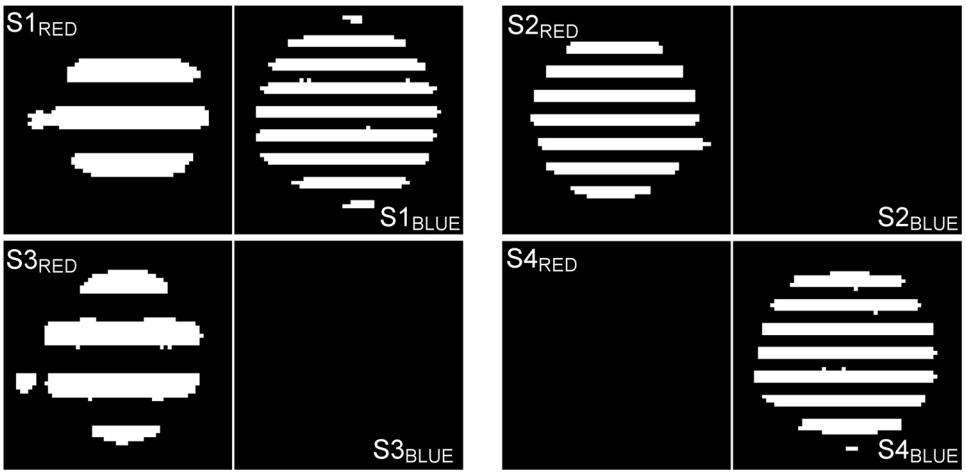

Fig. 9. Extracted binary images of the objects to be located for determining the corresponding source's code; the left image corresponds to the red channel while the right one represents the blue channel.

$$V_{\text{img}} = \begin{cases} \dfrac{2}{\varphi_V}\left[\tan^{-1}\dfrac{V_{\text{real}}}{2D + H_{\text{real}}\cos\gamma}\right] & ; \text{ Farthest elements} \\ \dfrac{2}{\varphi_V}\left[\tan^{-1}\dfrac{V_{\text{real}}}{2D - H_{\text{real}}\cos\gamma}\right] & ; \text{ Closest elements} \end{cases} \tag{3}$$

Since in this system all the beacons are located over a virtual plane, parallel to the camera's normal plane, the corresponding angle γ is equal to $\pi/2$ and Eqs. (2) and (3) can be simplified as shown in Eqs. (4) and (5) to find the real distances.

$$H_{\text{img}} = \frac{2}{\varphi_H}\left[\tan^{-1}\frac{H_{\text{real}}}{2D}\right] \Rightarrow H_{\text{real}} = 2D\cdot\left[\tan\frac{H_{\text{img}}\cdot\varphi_H}{2}\right] \tag{4}$$

$$V_{\text{img}} = \frac{2}{\varphi_V}\left[\tan^{-1}\frac{V_{\text{real}}}{2D}\right] \Rightarrow V_{\text{real}} = 2D\cdot\left[\tan\frac{V_{\text{img}}\cdot\varphi_V}{2}\right] \tag{5}$$

For each object, the distances OB_{Hi} and OB_{Vi}, shown in Fig 10 , are determined in pixels as $OB_{Hi} = |B_{Hi} - O_{Hi}|$ and $OB_{Vi} = |B_{Vi} - O_{Vi}|$ based on the data obtained during the image processing phase. Then these distances can be converted into real world lengths using Eqs. (4) and (5).

In the same way, the distance between the camera and the object to be located (D_O) can be estimated using Eq. (6) based on the relation between the projected diameters of each beacon (d_{Bi}) and the object (d_O).

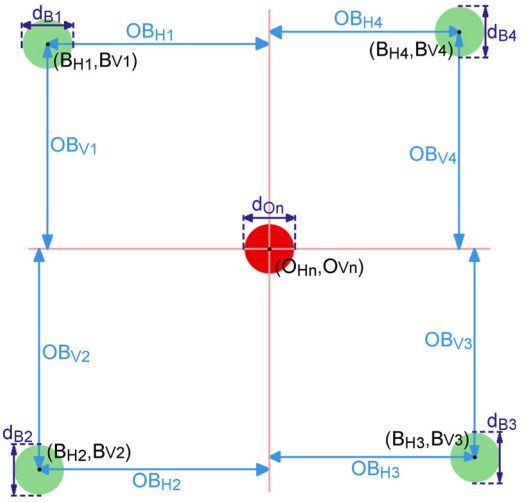

Fig. 10. Representation of the data obtained from the image processing phase for one object, highlighting the necessary distances for the localization process.

$$D_{Oi} = D \cdot \frac{\tan \frac{d_{Bi} \cdot \varphi_H}{2}}{\tan \frac{d_O \cdot \varphi_H}{2}} \tag{6}$$

Afterward, the distance from the object to each beacon (r_{OBi}) can be calculated by applying Eq. (7) and the object 3D location is obtained from simple trilateration, based on the known positions of the beacons.

$$r_{OBi} = \sqrt{OB_{Hi}^2 + OB_{Vi}^2 + (D - D_{Oi})^2} \tag{7}$$

2.4. Location management

Once the system finished the localization process of each object, the positioning data is stored. Depending on the implementation and defined applications of the system, these locations can be available to keep track of the objects' path. Additionally, the positions can be delivered to a central master device, so this equipment is able to control the objects according to their locations and targets. If the implementation has a peer-to-peer architecture, the positions can be transmitted directly to each device. This system allows the location data transmission through RF, or infro-red (IR) links.

3. Experimental validation

To demonstrate the viability of the proposed system, an experimental validation was performed. The tests for locating and tracking four objects at the same time were executed in a 3 m × 3.5 m × 2.5 m dark room. The selected emitter was a 16 cm^2 round shaped LEDs' arrange, composed by twelve 6-pin RGB LEDs with viewing angle of 120°. In this way, each color channel was independently controlled by a small single board computer programmed with Python; and each source emitted its unique identification signal as the OOK modulation of code '0 × AAAA' at the frequency and channel defined in Table 1.

For simplicity of the testing set up, all the emitters were stationed in different positions over a 2 m × 2 m × 2 cm board on the room's floor, parallel to the receiver's normal plane at a distance $D = 2.00$ m from the camera. The beacons (B_1–B_4) were kept in static positions, while the objects (O_1–O_4) were moved over a specific area of the room, as shown in Table 2.

The receiver was a COTS USB webcam with 640 × 480 pixels resolution and diagonal FOV of 78°, working at 30 fps. The camera was previously calibrated to avoid lenses' aberration and configured to assure contrast and low exposure time. The used configuration was: maximum contrast (255), no brightness (zero), manual average white balance (4000) and no autofocus. The webcam was software controlled to capture, store, and process the images.

At the beginning of the process, from the first stored frame, all the beacons were identified by associating the band's width $Npixels_i$ of the source with the corresponding beacon's line number. Additionally, the centroid' pixels location and the experimental diameter of the beacons, shown in Table 3, were obtained and stored for calculating the different positions of the objects.

As it has been done with the first frame, the following images were processed continuously to identify the objects and extract the sources' positioning data. As an example of the results of this image processing, in Table 4 the centroid's pixels location and the experimental diameter of the sources previously shown in Fig. 4 are presented, along with their corresponding identification.

These obtained measures were employed to estimate, for each object, the distances to the different beacons' horizontal and vertical positions and also the separation from the camera's normal plane. Then the 3D object's location was determined using trilateration. Table 5 presents the calculated positions of the objects showed in Fig. 4 based on the data from Table 4. For this selected example, the resolved positions showed a maximum error of 2.94 cm for x dimension, 3.04 cm for y dimension, and 0.93 cm for z dimension.

In each (x, y) position over the moving area of the objects, four 3D estimated locations were calculated, one per object. The position error range was between 0.16 cm and 3.10 cm for x dimension, between 0.09 cm and 2.65 cm for y dimension, and between 0.01 cm and 1.32 cm for z dimension. The average error position was appraised as a combination of these four measurements and the three dimensions. The corresponding error map from the experiments is shown in Fig. 11.

During the experiments, all the locations were stored in a database. Each data entry included the position, the device identification, and the time stamp. As a result of storing the values, the objects can be tracked independently or by a group. Moreover, queries to the database can be done using the object's identification, a time range or both parameters at the same time. As an example

Table 1
Emitter's characteristics.

Device ID	Frequency (Hz)	Colour channel
B_1	4800	Green
B_2	2400	Green
B_3	1200	Green
B_4	1800	Green
O_1	2400	Red
O_2	4800	Red
O_3	2400[a]/4800[b]	Red[a]/Blue[b]
O_4	4800	Blue

Table 2
Emitter's 3D positions.

Device	Position (m)		
ID	*x*	*y*	*z*
B_1	1.00	2.00	0.02
B_2	1.00	0.50	0.02
B_3	3.05	0.50	0.02
B_4	3.05	2.00	0.02
O_1–O_4	1.80–2.25	1.10–1.50	0.02

Table 3
Located Beacons' centroids data.

Beacons	Position (pixels)		Experimental
ID	Horizontal	Vertical	Diameter (pixels)
S1(B1)	25.28	29.13	43
S2(B2)	25.74	455.30	42.7
S3(B4)	615.24	27.00	42.9
S4(B3)	616.14	450.55	43

Table 4
Located objects' centroids data (example).

Source	Position (pixels)		Experimental
ID	Horizontal	Vertical	Diameter (pixels)
S1 (O3)	250.38	162.67	42.7
S2 (O2)	252.87	285.65	42.8
S3 (O1)	358.86	210.36	43.1
S4 (O4)	389.80	292.13	43.2

Table 5
Located objects' positions (example).

Source	Real Position (m)			Calculated Position (m)		
ID	*x*	*y*	*z*	*x*	*y*	*z*
O1	2.15	1.35	0.02	2.1646	1.3573	0.0109
O2	1.80	1.10	0.02	1.7802	1.0925	0.0156
O3	1.80	1.50	0.02	1.7706	1.5255	0.0247
O4	2.25	1.10	0.02	2.2772	1.0696	0.0293

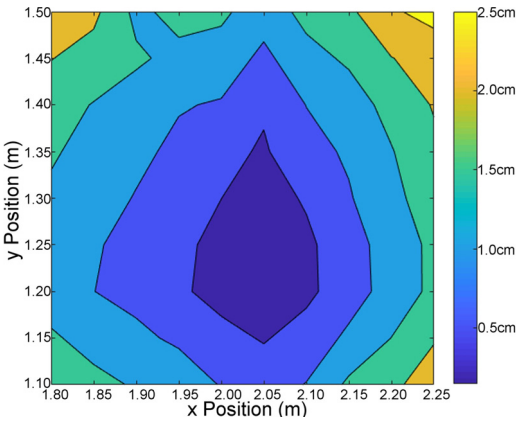

Fig. 11. Experiment's error map.

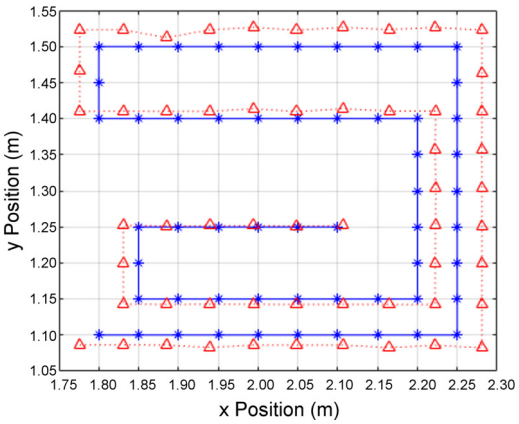

Fig. 12. Tracking experiment's results: the straight blue line represents the real path of the object, while the dotted red line constitutes the system track. (For interpretation of the references to color in this figure legend, the reader is referred to the web version of this article.)

of this process, Fig. 12 shows the movement tracking of object O_1 throughout 5 min. The straight blue line represents the real path of the object, which started on (1.80, 1.10) m and ended at (2.10, 1.25) m, while the dotted red line constitutes the system's track of the object. The maximum error location was 3.10 cm for x dimension, 2.65 cm for y dimension, and 0.48 cm for z dimension.

4. Conclusions

This work has demonstrated that a real-time two-step 3D indoor localization system based on OCC for multiple simultaneous objects is feasible. This OCC indoor localization system can be easily implemented for robots' navigation in the emerging Industrial Internet of Things (IIoT) applications field, or any tracking execution, since the proposed scheme does not require an embedded camera in the objects to be located.

During the laboratory experiment, four objects were accurately positioned and tracked. For a distance of $D = 2.00$ m, with a camera resolution of 640 × 480 pixels and FOV angle of 78° the average location error obtained was 1.2434 cm, with an average process time of 18.2 ms per frame. In the same way, the tracking phase of the system was proved for object O_1 with a mean error of 1.07 cm over a 5 min lapse.

Since in a photo each pixel represents a specific real distance, which value is based on the distance between the object and the image sensor, and the camera's characteristics (resolution and FOV), the position accuracy of this system depends on those parameters. It is directly proportional to the resolution and inversely proportional to the camera's FOV and the distance. For example, for a camera with 640 × 480 pixels resolution and 78° FOV, like the one used in these experiments, at 2.00 m each pixel represents 3.40 mm, while at 4.00 m corresponds to 6.80 mm. In this way, an error of one pixel in the image processing stage will lead to an additional location error of 3.40 mm for a distance of 2.00 m and will duplicate the value for 4.00 m.

In future works, the problem of covering the entire room will be taken into account. More locating and tracking experiments will be held using several objects and multiple cameras with overlapping view's range. In the same way, the identifying signals of all the devices will be transmitted using the three channels to increase the number of simultaneous objects to be located and to study the hand-off process between the cameras.

Acknowledgements

This work was supported in part by Escuela Superior Politecnica del Litoral, Ecuador. This work was also supported by the Spanish Government as a part of the Spanish Research Administration (MICIU project: OSCAR, ref.: TEC 2017-84065-C3-1-R).

References

[1] P. Misra, P. Enge, Global Positioning System: Signals, Measurements, and Performance, Ganga – JamunaPress, USA, 2006.
[2] B. Li, J. Salter, A.G. Dempster, C. Rizos, Indoor positioning techniques based on wireless lan, First IEEE International Conference on Wireless Broadband and Ultra Wideband Communications, IEEE, Sydney, Australia, 2006, pp. 13–16.
[3] M. Bouet, A.L. dos Santos, RFID tags: positioning principles and localization techniques, 2008 1st IFIP Wireless Days, IEEE, 2008, pp. 1–5, https://doi.org/10.1109/WD.2008.4812905.
[4] IEEE Standard for Local and Metropolitan Area Networks-Part 15.7: Short-Range Wireless Optical Communication Using Visible Light, 2011 https://doi.org/doi: 10.1109/IEEESTD.2011.6016195.
[5] M.F. Keskin, A.D. Sezer, S. Gezici, Localization via visible light systems, Proc. IEEE 106 (2018) 1063–1088.
[6] G. Kail, P. Maechler, N. Preyss, A. Burg, Robust asynchronous indoor localization using led lighting, 2014 IEEE International Conference on Acoustics, Speech and Signal Processing (ICASSP), IEEE, 2014, pp. 1866–1870, https://doi.org/10.1109/ICASSP.2014.6853922.
[7] H. Steendam, T.Q. Wang, J. Armstrong, Cramer-Rao bound for indoor visible light positioning using an aperture-based angular-diversity receiver, 2016 IEEE International Conference on Communications (ICC) (2016) 1–6, https://doi.org/10.1109/ICC.2016.7510822.
[8] I. Marin-Garcia, P. Chavez-Burbano, A. Munoz-Arcentles, V. Calero-Bravo, R. Perez-Jimenez, Indoor location technique based on visible light communications

and ultrasound emitters, 2015 IEEE International Conference on Consumer Electronics (ICCE), Institute of Electrical and Electronics Engineers (IEEE), 2015, pp. 297–298, https://doi.org/10.1109/ICCE.2015.7066421.
[9] E. Torres-Zapata, J.M. Luna-Rivera, R. Perez-Jimenez, V. Guerra, J. Rabadan, J. Rufo, C.A. Gutierrez, Implementation of a VLC-based indoor localization system, Trans. Emerg. Telecommun. Technol. (2018) e3498.
[10] T.-H. Do, M. Yoo, An in-depth survey of visible light communication based positioning systems, Sensors 16 (2016) 678.
[11] M.T. Taylor, S. Hranilovic, Angular diversity approach to indoor positioning using visible light, 2013 IEEE Globecom Workshops (GC Wkshps) (2013) 1093–1098, https://doi.org/10.1109/GLOCOMW.2013.6825138.
[12] S.H. Yang, D.R. Kim, H.S. Kim, Y.H. Son, S.K. Han, Indoor positioning system based on visible light using location code, 2012 Fourth International Conference on Communications and Electronics (ICCE) (2012) 360–363, https://doi.org/10.1109/CCE.2012.6315928.
[13] S.-H. Yang, D.-R. Kim, H.-S. Kim, Y.-H. Son, S.-K. Han, Visible light based high accuracy indoor localization using the extinction ratio distributions of light signals, Microw. Optic. Technol. Lett. 55 (2013) 1385–1389.
[14] T.Q. Wang, Y.A. Sekercioglu, A. Neild, J. Armstrong, Position accuracy of time-of-arrival based ranging using visible light with application in indoor localization systems, J. Light. Technol. 31 (2013) 3302–3308.
[15] P. Luo, M. Zhang, X. Zhang, G. Cai, D. Han, Q. Li, An indoor visible light communication positioning system using dual-tone multi-frequency technique, 2013 2nd International Workshop on Optical Wireless Communications (IWOW) (2013) 25–29, https://doi.org/10.1109/IWOW.2013.6777770.
[16] P. Luo, Z. Ghassemlooy, H.L. Minh, A. Khalighi, X. Zhang, M. Zhang, C. Yu, Experimental demonstration of an indoor visible light communication positioning system using dual-tone multi-frequency technique, 2014 3rd International Workshop in Optical Wireless Communications (IWOW), IEEE, 2014, pp. 55–59, https://doi.org/10.1109/IWOW.2014.6950776.
[17] M. Biagi, S. Pergoloni, A.M. Vegni, Last: a framework to localize, access, schedule, and transmit in indoor vlc systems, J. Light. Technol. 33 (2015) 1872–1887.
[18] D. Zheng, G. Chen, J.A. Farrell, Navigation using linear photo detector arrays, 2013 IEEE International Conference on Control Applications (CCA) (2013) 533–538, https://doi.org/10.1109/CCA.2013.6662804.
[19] Indoor location measuring device and method, 2012. https://www.google.es/patents/WO2012008650A1?cl=en, wO Patent App. PCT/KR2010/005,779.
[20] Y.-S. Kuo, P. Pannuto, K.-J. Hsiao, P. Dutta, Luxapose: indoor positioning with mobile phones and visible light, Proceedings of the 20th Annual International Conference on Mobile Computing and Networking, MobiCom'14, ACM, New York, NY, USA, 2014, pp. 447–458, https://doi.org/10.1145/2639108.2639109.
[21] M.S. Ifthekhar, N. Saha, Y.M. Jang, Neural network based indoor positioning technique in optical camera communication system, 2014 International Conference on Indoor Positioning and Indoor Navigation (IPIN), IEEE, 2014, pp. 431–435, https://doi.org/10.1109/IPIN.2014.7275513.
[22] Z. Yang, Z. Wang, J. Zhang, C. Huang, Q. Zhang, Wearables can afford: light-weight indoor positioning with visible light, Proceedings of the 13th Annual International Conference on Mobile Systems, Applications, and Services, MobiSys'15, ACM, New York, NY, USA, 2015, pp. 317–330, https://doi.org/10.1145/2742647.2742648.
[23] P. Huynh, M. Yoo, VLC-based positioning system for an indoor environment using an image sensor and an accelerometer sensor, Sensors 16 (2016) 783.
[24] R. Zhang, W.-D. Zhong, D. Wu, K. Qian, A novel sensor fusion based indoor visible light positioning system, 2016 IEEE Globecom Workshops (GC Wkshps), IEEE, 2016, pp. 1–6, https://doi.org/10.1109/GLOCOMW.2016.7848823.
[25] B. Lin, Z. Ghassemlooy, C. Lin, X. Tang, Y. Li, S. Zhang, An indoor visible light positioning system based on optical camera communications, IEEE Photonics Technol. Lett. 29 (2017) 579–582.
[26] C. Lin, B. Lin, X. Tang, Z. Zhou, H. Zhang, S. Chaudhary, Z. Ghassemlooy, An indoor visible light positioning system using artificial neural network, 2018 Asia Communications and Photonics Conference (ACP), IEEE, 2018, pp. 1–3, https://doi.org/10.1109/ACP.2018.8596227.
[27] P. Chavez-Burbano, V. Guerra, J. Rabadan, C. Jurado-Verdu, R. Perez-Jimenez, Novel indoor localization system using optical camera communication, 2018 11th International Symposium on Communication Systems, Networks Digital Signal Processing (CSNDSP), IEEE, 2018, pp. 1–5, https://doi.org/10.1109/CSNDSP.2018.8471774.
[28] N. Otsu, A threshold selection method from gray-level histograms, IEEE Trans. Syst. Man Cybern. 9 (1979) 62–66.
[29] P. Chavez-Burbano, V. Guerra, J. Rabadan, D. Rodríguez-Esparragón, R. Perez-Jimenez, Experimental characterization of close-emitter interference in an optical camera communication system, Sensors 17 (2017) 1561.